Weierstraß–Institut
für Angewandte Analysis und Stochastik

im Forschungsverbund Berlin e.V.

Preprint ISSN 0946 – 8633

A Transient Model for the Sublimation Growth of Silicon Carbide Single Crystals

N. Bubner, O. Klein, P. Philip, J. Sprekels, K. Wilmański

submitted: 21 Oct 1998

Weierstraß–Institut für Angewandte Analysis und Stochastik, Mohrenstraße 39, 10117 Berlin, Germany

Preprint No. 443
Berlin 1998

1991 Mathematics Subject Classification. 80A20, 65M99, 80A15, 65C20, 35L65.

Key words and phrases. Modelling, sublimation growth, heat and mass transfer, numerical simulation, conservation laws, partial differential equations.

1998 PACS numbers. 81.10.Bk, 82.20.Wt, 44.90.+c, 83.10.Ff.

Edited by
Weierstraß–Institut für Angewandte Analysis und Stochastik (WIAS)
Mohrenstraße 39
D — 10117 Berlin
Germany

Fax: + 49 30 2044975
E-Mail (X.400): c=de;a=d400-gw;p=WIAS-BERLIN;s=preprint
E-Mail (Internet): preprint@wias-berlin.de
World Wide Web: http://www.wias-berlin.de/

Abstract

We present a transient model for the *Modified Lely Method* for the sublimation growth of SiC single crystals which consists of all conservation laws including reaction–diffusion equations. The model is based on a mixture theory for the gas phase. First numerical results illustrate the influence of the geometrical set–up inside the reactor on the evolution of the temperature distribution.

1 Introduction

SiC single crystals have received rapidly growing attention in recent years due to the wide range of their current industrial applications. There is an increasing use of these crystals in electronic and optoelectronic devices, such as semiconductors and lasers, especially when high power, high frequency, intensive radiation, or high temperature is involved.

Looking for crystals with a low defect rate and large in dimension, the most promising production method of recent years has been the so–called *Modified Lely Method*. Inside a heated graphite crucible polycrystalline SiC powder is evaporated, and a single crystal grows on a cooled seed via sublimation. This very complex process will be discussed below in greater detail.

The crucible is not accessible to direct observation due to temperatures of up to 3000 K, and only very few indirect measurements can be carried out to control the experiments. Hence, numerical simulations are necessary in order to better understand the involved physical and chemical phenomena, to control the production and to improve quality and size of the crystals. There is a number of publications dealing with this task, e.g. [Lil93], [HHW$^+$95], [Kon95], and [PBD$^+$96]. We think, however, that none of these papers takes all relevant physical properties of the concerned method into account. In particular, to the authors' knowledge, only stationary models exist in the literature.

The aim of our present and future work is to develop a model including all relevant phenomena of the sublimation growth process. We underline the fact that we deal with a *transient* model. The development of a transient model is considered to be essential, since time dependence appears to be one of the most crucial intrinsic properties of the method. In the sequel, we describe the production method more precisely.

As temperatures of some 3000 K are necessary for the growth process to occur, only a graphite crucible can be used as reactor. The inner part of the actual reactor exhibits a quite complicated structure which consists of cavities and of several materials, such as different sorts of graphite, SiC in various modifications, and others. The optimal inner structure is not yet known, and it is one goal of the numerical simulations to determine it. In the center of the crucible we have the reaction chamber with the SiC powder on the bottom and the seed on the top (cf. Figure 1). We consider induction heating which induces eddy currents in the outer part of the reactor. The Joule effect then heats the crucible. The heat is transported to the center of the reactor via radiation through the cavities and via conduction through the different materials. The evaporation of the source, i.e. of the SiC powder, creates a gas mixture in the reaction chamber. Since the seed is cooled by a blind hole at the top of the crucible, the crystal grows downwards into the reaction chamber via sublimation of the gas due to chemical reactions.

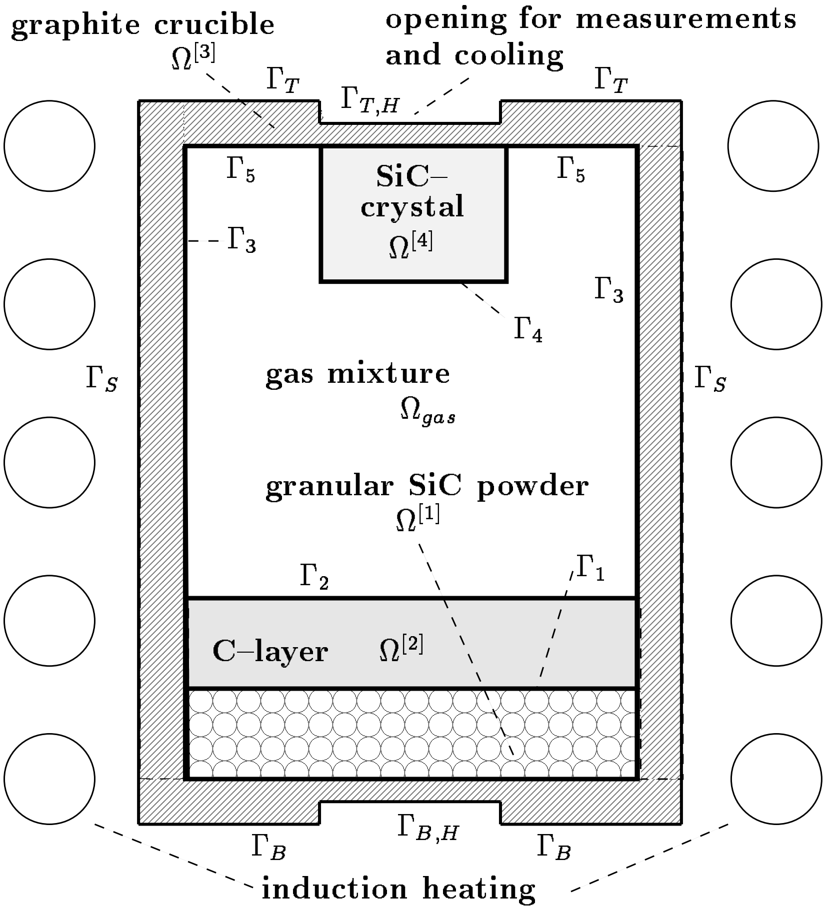

Figure 1: Draft of the growth chamber.

One uses argon as inert gas inside the reactor. In addition to argon, the gas is made up of several species, such as Si, SiC, Si_2C, SiC_2, and C. One of the most complicated issues in the process is the occurrence of chemical reactions between these gas species in the gas phase itself, on the source, on the graphite walls, and on the surface of the growing crystal. Clearly, one has to model these chemical reactions in order to simulate the crystal growth, and here time is playing an important role. The stoichiometry of the gas species is changing with the course of time from the following reasons: Si is leaking out of the porous graphite reaction chamber, C is closing the pores of the walls and covering the source, and the source is sintering and changing its evaporation rate.

The distance between the source and the crystal is of great importance. Since it changes permanently during the whole procedure, this is another crucial point where time dependence is involved. In addition, as the temperature field is not constant in the reaction chamber but very significant for the crystal growth, one ought to aim at optimizing the temperature field during the whole process corresponding to the growing crystal.

Furthermore, experiments show that the quality of the crystal strongly depends on the initial conditions (cf. [Ins97]). It is therefore necessary to simulate the initial phase of the process, i.e. the time period when the reactor is heated up from room temperature to actual growth conditions.

To account for all the aforementioned aspects is a difficult task and not yet finished. Nevertheless, a first step has come to a conclusion. The next section will present the current state of our model. So far, all conservation laws including reaction–diffusion–equations for the gas mixture as well as the energy balance for the entire reactor are considered. In Section 3 we will report first numerical results. Further modeling and corresponding numerical simulations will be the subject of forthcoming papers.

2 The Model

In Section 2.1, we consider the model of the gas mixture in the reaction chamber. Subsequently, modeling of the solid parts of the growth apparatus is done in Section 2.2. Boundary and interface conditions are discussed in Section 2.3. Certain aspects of future improvements are mentioned where appropriate.

At the present state of the model, the evolution of velocity, density, and concentration of the gas species inside the reaction chamber as much as the temperature distribution inside and outside the gas phase is determined for a given configuration of the reactor, where the position of the surface of the crystal and of the SiC–powder are fixed. Models for the growth of the crystal and the sintering of the SiC–powder are presently under work.

2.1 Model of the Gas Mixture

In the domain of the gas mixture (Ω_{gas}, cf. Figure 1), one has to deal with the interchange of mass and momentum between the different components in addition to chemical reactions and thermo–mechanical processes such as motion and heat transport. To model this situation, we use continuous mixture theory and make some simplifications that are valid by experimentally known properties (cf. [Ins97]).

Let the gas mixture consist of A components, denoted by the superscript (α). In practice, the essential components are Ar, SiC, Si, SiC_2, Si_2C, and C. For each component the following conservation laws hold:

- mass:

$$\frac{\partial \rho^{(\alpha)}}{\partial t} + \operatorname{div}\left(\rho^{(\alpha)}\vec{v}^{\,(\alpha)}\right) = \rho^{*(\alpha)}; \tag{2.1a}$$

- momentum:

$$\frac{\partial\left(\rho^{(\alpha)}\vec{v}^{\,(\alpha)}\right)}{\partial t} + \operatorname{div}\left(\rho^{(\alpha)}\vec{v}^{\,(\alpha)} \otimes \vec{v}^{\,(\alpha)} - \underset{\sim}{T}^{(\alpha)}\right) = \vec{m}^{*(\alpha)} + \rho^{(\alpha)}\vec{b}^{\,(\alpha)}; \tag{2.1b}$$

- energy:

$$
\begin{aligned}
&\frac{\partial}{\partial t}\left(\rho^{(\alpha)}\left(\varepsilon^{(\alpha)}+\frac{1}{2}\left(\vec{v}^{(\alpha)}\right)^2\right)\right)\\
&+\operatorname{div}\left(\rho^{(\alpha)}\left(\varepsilon^{(\alpha)}+\frac{1}{2}\left(\vec{v}^{(\alpha)}\right)^2\right)\vec{v}^{(\alpha)}+\vec{q}^{(\alpha)}-\underset{\sim}{T}^{(\alpha)}\vec{v}^{(\alpha)}\right)\\
&=\rho^{(\alpha)}\vec{b}^{(\alpha)}\bullet\vec{v}^{(\alpha)}+\rho^{(\alpha)}r^{(\alpha)}.
\end{aligned}
\tag{2.1c}
$$

Here we have used the notation

$\rho^{(\alpha)}$ – partial mass density, $\vec{v}^{(\alpha)}$ – partial velocity,
$\underset{\sim}{T}^{(\alpha)}$ – partial stress tensor, $\vec{m}^{*(\alpha)}$ – diffusion force density,
$\vec{b}^{(\alpha)}$ – mass force density (e.g. gravity),
$\varepsilon^{(\alpha)}$ – partial internal energy, $\vec{q}^{(\alpha)}$ – partial heat flux,
$r^{(\alpha)}$ – partial radiation, $\rho^{*(\alpha)}$ – partial mass source (chemical reactions, phase transitions).

The componentwise conservation laws are completed by the global conservation laws

$$\sum_{\alpha=1}^{A}\vec{m}^{*(\alpha)}=0, \qquad \sum_{\alpha=1}^{A}\rho^{*(\alpha)}=0. \tag{2.2}$$

At any given time the state of the gas mixture is determined by the $2A+1$ quantities

$$\left\{\ \rho^{(1)},\rho^{(2)},\dots,\rho^{(A)},\ \ \vec{v}^{(1)},\vec{v}^{(2)},\dots,\vec{v}^{(A)},\ \ T_{gas}\ \right\}, \tag{2.3}$$

where T_{gas} denotes the absolute temperature.
Alternatively, this also holds for the $2A+3$ quantities

$$\left\{\ \rho_{gas},\ \vec{v}_{gas},\ c^{(1)},c^{(2)},\dots,c^{(A)},\ \vec{u}^{(1)},\vec{u}^{(2)},\dots,\vec{u}^{(A)},\ T_{gas}\ \right\}, \tag{2.4}$$

where

$$\rho_{gas} := \sum_{\alpha=1}^{A}\rho^{(\alpha)}, \qquad \rho_{gas}\vec{v}_{gas} := \sum_{\alpha=1}^{A}\rho^{(\alpha)}\vec{v}^{(\alpha)}, \tag{2.5a}$$

$$c^{(\alpha)} := \frac{\rho^{(\alpha)}}{\rho_{gas}}, \qquad \vec{u}^{(\alpha)} := \vec{v}^{(\alpha)}-\vec{v}_{gas}, \quad \alpha=1,\dots,A. \tag{2.5b}$$

Here, ρ_{gas} is the density of the gas mixture, $\vec{v}_{gas}$ is the average velocity of all components, $c^{(\alpha)}$ is the concentration, and $\vec{u}^{(\alpha)}$ is the diffusion velocity of the component α. Note that

$$\sum_{\alpha=1}^{A}c^{(\alpha)}=1, \qquad \sum_{\alpha=1}^{A}c^{(\alpha)}\vec{u}^{(\alpha)}=0. \tag{2.6}$$

By using the conservation laws (2.1) and (2.2), one finds that the quantities (2.4) satisfy the following system of equations

$$\frac{d\rho_{gas}}{dt} + \rho_{gas}\,\mathrm{div}\,\vec{v}_{gas} = 0, \tag{2.7a}$$

$$\frac{dc^{(\alpha)}}{dt} + \frac{1}{\rho_{gas}}\,\mathrm{div}\left(\rho_{gas} c^{(\alpha)} \vec{u}^{\,(\alpha)}\right) = \frac{1}{\rho_{gas}}\,\rho^{*(\alpha)}, \tag{2.7b}$$

$$\rho_{gas}\frac{d\vec{v}_{gas}}{dt} = \mathrm{div}\,\underset{\sim}{T} + \rho_{gas}\vec{b}_{gas}, \tag{2.7c}$$

$$\begin{aligned} & c^{(\alpha)}\frac{d\vec{u}^{\,(\alpha)}}{dt} + \left(\mathrm{grad}\left(\vec{u}^{\,(\alpha)} + \vec{v}_{gas}\right)\right)\ \left(c^{(\alpha)}\vec{u}^{\,(\alpha)}\right) \\ & = \frac{1}{\rho_{gas}}\left(\mathrm{div}\,\underset{\sim}{T}^{(\alpha)} - c^{(\alpha)}\,\mathrm{div}\,\underset{\sim}{T}\right) \\ & \quad + \frac{1}{\rho_{gas}}\left(\vec{m}^{*(\alpha)} - \rho^{*(\alpha)}\vec{v}^{\,(\alpha)}\right) + c^{(\alpha)}\left(\vec{b}^{\,(\alpha)} - \vec{b}_{gas}\right), \end{aligned} \tag{2.7d}$$

$$\frac{d\varepsilon_{gas}}{dt} + \frac{1}{\rho_{gas}}\,\mathrm{div}\,\vec{q}_{gas} = \frac{1}{\rho_{gas}}\ \underset{\sim}{T} \bullet \mathrm{grad}\,\vec{v}_{gas} + r_{gas}, \tag{2.7e}$$

where

$$\frac{d}{dt} := \frac{\partial}{\partial t} + \vec{v}_{gas} \bullet \mathrm{grad}, \tag{2.8a}$$

$$\underset{\sim}{T} := \sum_{\alpha=1}^{A}\left(\underset{\sim}{T}^{(\alpha)} - \rho^{(\alpha)}\vec{u}^{\,(\alpha)} \otimes \vec{u}^{\,(\alpha)}\right), \tag{2.8b}$$

$$\rho_{gas}\,\vec{b}_{gas} := \sum_{\alpha=1}^{A} \rho^{(\alpha)}\vec{b}^{\,(\alpha)}, \tag{2.8c}$$

$$\rho_{gas}\,\varepsilon_{gas} := \sum_{\alpha=1}^{A} \rho^{(\alpha)}\left(\varepsilon^{(\alpha)} + \frac{1}{2}\left(\vec{u}^{\,(\alpha)}\right)^2\right), \tag{2.8d}$$

$$\rho_{gas}\,r_{gas} := \sum_{\alpha=1}^{A} \rho^{(\alpha)}\left(r^{(\alpha)} + \vec{b}^{\,(\alpha)} \bullet \vec{u}^{\,(\alpha)}\right), \tag{2.8e}$$

$$\vec{q}_{gas} := \sum_{\alpha=1}^{A}\left(\vec{q}^{\,(\alpha)} + \rho^{(\alpha)}\varepsilon^{(\alpha)}\vec{u}^{\,(\alpha)} - \underset{\sim}{T}^{(\alpha)}\vec{u}^{\,(\alpha)} + \frac{1}{2}\rho^{(\alpha)}\left(\vec{u}^{\,(\alpha)}\right)^2\vec{u}^{\,(\alpha)}\right). \tag{2.8f}$$

Now, we are going to simplify the system (2.7)–(2.8).

As usual, we assume the existence of diffusion coefficients $D^{(\alpha,\beta)} = D^{(\alpha,\beta)}(c^{(\alpha)}, c^{(\beta)}, T_{gas})$

such that

$$\begin{aligned}
\vec{m}^{*(\alpha)} \; - \; \rho^{*(\alpha)}\vec{v}^{\,(\alpha)} &= -\sum_{\beta=1}^{A} D^{(\alpha,\beta)}\vec{u}^{\,(\beta)} \\
&= -\sum_{\beta=1}^{A} D^{(\alpha,\beta)}\left(\vec{u}^{\,(\beta)} - \vec{u}^{\,(\alpha)}\right) - \sum_{\beta=1}^{A} D^{(\alpha,\beta)}\vec{u}^{\,(\alpha)} \\
&= -\sum_{\beta=1}^{A} D^{(\alpha,\beta)}\left(\vec{u}^{\,(\beta)} - \vec{u}^{\,(\alpha)}\right) - D^{(\alpha)}\vec{u}^{\,(\alpha)}, \quad \alpha = 1,\ldots,A, \qquad (2.9)
\end{aligned}$$

where $D^{(\alpha)} := \sum_{\beta=1}^{A} D^{(\alpha,\beta)}$. We assume further that only the second term in (2.9) has to be taken into account, i.e.

$$\vec{m}^{*(\alpha)} - \rho^{*(\alpha)}\vec{v}^{\,(\alpha)} = -D^{(\alpha)}(c^{(1)},\ldots,c^{(A)},T_{gas})\,\vec{u}^{\,(\alpha)}, \quad \alpha = 1,\ldots,A. \qquad (2.10)$$

In addition, we suppose that the partial stress tensor is of the form

$$-\underset{\sim}{T}^{(\alpha)} = p^{(\alpha)}\,\underset{\sim}{1}, \quad \alpha = 1,\ldots,A, \qquad (2.11)$$

where $p^{(\alpha)}$ denotes the partial pressure.

The diffusion processes are supposed to change slowly in time, i.e.

$$\frac{d\vec{u}^{\,(\alpha)}}{dt} \approx 0, \quad \alpha = 1,\ldots,A. \qquad (2.12)$$

The only mass force present is the gravity $\vec{g}$, i.e.

$$\vec{b}^{\,(\alpha)} = \vec{g}, \quad \alpha = 1,\ldots,A. \qquad (2.13)$$

Taking into account the high temperature and the low pressure (≈ 20 hPa) of the gas in the reaction chamber, one can assume that the gas mixture is essentially an ideal gas. Hence, for the component α the material laws read

$$p^{(\alpha)} = \rho_{gas}c^{(\alpha)}\frac{R}{M^{(\alpha)}}T_{gas}, \qquad (2.14a)$$

$$\varepsilon^{(\alpha)} = z^{(\alpha)}\frac{R}{M^{(\alpha)}}T_{gas}, \qquad (2.14b)$$

$$\vec{q}^{\,(\alpha)} = -\kappa^{(\alpha)}\left(c^{(\alpha)},T_{gas}\right)\operatorname{grad}T_{gas}, \qquad (2.14c)$$

$$\rho^{*(\alpha)} = \sum_{i=1}^{N} \gamma_i^{(\alpha)}\, M^{(\alpha)}\, \mu_H\, \Lambda^{(i)}\left(c^{(1)},\ldots,c^{(A)}\right), \qquad (2.14d)$$

where R is the universal gas constant, $M^{(\alpha)}$ is the molecular weight, $z^{(\alpha)} = \frac{3}{2}$ for single–, $z^{(\alpha)} = \frac{5}{2}$ for double–, and $z^{(\alpha)} = 3$ for multi–atomic gas molecules, $\kappa^{(\alpha)}$ is the heat conductivity, N is the number of chemical reactions and phase transitions, $\gamma_i^{(\alpha)}$

are the stoichiometric coefficients, μ_H is the hydrogen molecular weight, and $\Lambda^{(i)}$ are rates of chemical reactions or phase transitions, respectively.

In the light of experimentally known material data (cf. [Ins97]) and estimated values for the velocity, one arrives at the following estimates:

$$\frac{1}{2}\rho^{(\alpha)}\left(\vec{u}^{\,(\alpha)}\right)^2 \ll p^{(\alpha)}, \qquad \rho^{(\alpha)}\sum_{i,j=1}^{3}\left|\left(\vec{u}^{\,(\alpha)}\otimes\vec{u}^{\,(\alpha)}\right)_{i,j}\right| \ll p^{(\alpha)}, \tag{2.15a}$$

$$\frac{1}{2}\left(\vec{u}^{\,(\alpha)}\right)^2 \ll \varepsilon^{(\alpha)}, \qquad \rho^{(\alpha)}\left\|\vec{u}^{\,(\alpha)}\bullet\operatorname{grad}\left(\vec{u}^{\,(\alpha)}+\vec{v}_{gas}\right)\right\| \ll \left\|\operatorname{grad}p^{(\alpha)}\right\|, \tag{2.15b}$$

where $\|\cdot\|$ denotes the usual Euclidean metric on $\mathbb{R}^3$. The terms on the left–hand sides will henceforth be neglected.

Thanks to these simplifications, equation (2.7d) for the diffusion velocity of the components leads to

$$\operatorname{grad}p^{(\alpha)} - c^{(\alpha)}\operatorname{grad}p_{gas} = -D^{(\alpha)}\,\vec{u}^{\,(\alpha)}, \quad \alpha = 1,\ldots,A, \tag{2.16}$$

where p_{gas} denotes the total pressure of the gas mixture, i.e.

$$p_{gas} := \sum_{\alpha=1}^{A} p^{(\alpha)}. \tag{2.17}$$

By (2.16), we can eliminate the quantity $\vec{u}^{\,(\alpha)}$ from the system (2.7).

Thus, the balance equations take the form

$$\text{mass:} \qquad \frac{d\rho_{gas}}{dt} + \rho_{gas}\operatorname{div}\vec{v}_{gas} = 0, \tag{2.18a}$$

$$\text{momentum:} \qquad \rho_{gas}\frac{d\vec{v}_{gas}}{dt} + \operatorname{grad}p_{gas} = \rho_{gas}\,\vec{b}_{gas}, \tag{2.18b}$$

$$\text{energy:} \qquad \frac{d\varepsilon_{gas}}{dt} + \frac{1}{\rho_{gas}}\operatorname{div}\vec{q}_{gas} + \frac{1}{\rho_{gas}}\,p_{gas}\operatorname{div}\vec{v}_{gas} = r_{gas}, \tag{2.18c}$$

completed by the reaction–diffusion equations

$$\begin{aligned}&\frac{dc^{(\alpha)}}{dt} - \frac{1}{\rho_{gas}}\operatorname{div}\left(\rho_{gas}c^{(\alpha)}\left(D^{(\alpha)}\right)^{-1}\left(\operatorname{grad}p^{(\alpha)} - c^{(\alpha)}\operatorname{grad}p_{gas}\right)\right)\\ &= \frac{1}{\rho_{gas}}\,\rho^{*(\alpha)}, \quad \alpha = 1,\ldots,A.\end{aligned} \tag{2.18d}$$

In these equations, the respective quantities defined in (2.8) simplify to

$$\vec{b}_{gas} = \vec{g}, \quad \varepsilon_{gas} = \sum_{\alpha=1}^{A} c^{(\alpha)}\varepsilon^{(\alpha)}, \quad r_{gas} = \sum_{\alpha=1}^{A} c^{(\alpha)}r^{(\alpha)}, \tag{2.19a}$$

$$\vec{q}_{gas} = \sum_{\alpha=1}^{A}\left(\vec{q}^{\,(\alpha)} - \left(\rho_{gas}c^{(\alpha)}\varepsilon^{(\alpha)} + p^{(\alpha)}\right)\left(D^{(\alpha)}\right)^{-1}\left(\operatorname{grad}p^{(\alpha)} - c^{(\alpha)}\operatorname{grad}p_{gas}\right)\right). \tag{2.19b}$$

The full system of equations for the quantities $\left\{ \rho_{gas},\ \ \vec{v}_{gas},\ \ c^{(1)}, c^{(2)}, \ldots, c^{(A)},\ \ T_{gas} \right\}$ consists of the $A+5$ scalar partial differential equations (2.18), coupled by (2.19), the material laws (2.14), material functions for $D^{(\alpha)}$, $\kappa^{(\alpha)}$, $\Lambda^{(i)}$, and some appropriate ansatz for the partial radiation $r^{(\alpha)}$.

We assume that almost no radiation is emitted or absorbed by the gas. This assumption seems to be justified since the gas components involved do not have any absorption or emission lines in their spectra in the range of the interesting temperatures (cf. [Ins97]). Hence, the radiation emitted by the gas can be neglected compared to that emitted by the surfaces of the solid components of the crucible. However, it is still an open question whether the absorption of radiation by the gas has to be taken into account in the energy balance for the gas.

2.2 Heat Transport in the Solid Parts of the Growth Apparatus

The growth apparatus consists of several solid components referred to by the superscript $[\beta]$. Some of the components are porous media, but at the current stage of modeling, we consider all solid component parts as non–porous.

Moreover, we do not consider any mechanical or chemical effects inside the solid components. Hence, the energy balance for the component β is given by

$$\rho^{[\beta]} \frac{\partial \left(c_{sp}^{[\beta]} \left(T^{[\beta]}\right) T^{[\beta]} \right)}{\partial t} + \operatorname{div} \vec{q}^{\,[\beta]} = \rho^{[\beta]} \mu^{[\beta]} \left(T^{[\beta]}, \vec{x}\right) \quad \text{in} \quad \Omega^{[\beta]}. \tag{2.20}$$

Here, $\Omega^{[\beta]}$ is the corresponding spatial domain, $\rho^{[\beta]}$ is the mass density, $c_{sp}^{[\beta]}$ is the specific heat, $T^{[\beta]}$ is the absolute temperature, $\vec{q}^{\,[\beta]} = -\kappa^{[\beta]}(T^{[\beta]}) \operatorname{grad} T^{[\beta]}$ is the heat flux, $\kappa^{[\beta]}$ is the heat conductivity, $\mu^{[\beta]}(T^{[\beta]}, \vec{x})$ is a heat source corresponding to the induction heating, and $\vec{x}$ is the space variable.

2.3 Boundary and Interface Conditions

At the boundaries $\Gamma_T, \Gamma_S, \Gamma_B$, we use appropriate boundary conditions of 1st, 2nd, or 3rd kind for the temperature.

At the boundaries $\Gamma_{T,H}$ and $\Gamma_{B,H}$, the emission of radiation is considered by using the Stefan–Boltzmann law. This leads to the condition

$$\vec{q}^{\,[3]} \bullet \vec{n} = \sigma \varepsilon^{[3]} \left(T^{[3]}\right) \left(T^{[3]}\right)^4 \quad \text{on} \quad \Gamma_{T,H} \cup \Gamma_{B,H}, \tag{2.21}$$

where $\vec{n}$ denotes the outer unit normal vector with respect to $\Omega^{[3]}$, σ denotes the Stefan–Boltzmann radiation constant, and $\varepsilon^{[3]}$ denotes the emissivity of graphite.

Heat flux and temperature are continuous at all interfaces.

In the current stage of modeling, we suppose a zero flux and and non–gliding condition on Ω_{gas}, i.e.

$$\vec{v}^{\,(\alpha)} = 0 \quad \text{on} \quad \partial\Omega_{gas}, \quad \alpha = 1, \ldots, A. \tag{2.22}$$

In a later stage of modeling, this assumption will be replaced by a more complicated condition involving also the internal and external pressures. The interface conditions for temperature and heat flux will than have to be adapted, as well.

Moreover, in a later stage, the boundaries Γ_1, Γ_2, and Γ_4 will be considered as moving boundaries, where the movement of the interface and the evolution of temperature, density, velocity, and concentrations will be highly nonlinearly coupled. This is an important step to model the growth of the crystal.

3 Numerical Simulation

3.1 Simplifications for the Numerical Treatment

For the first stages of the numerical simulation, we will deal with the mass and momentum balance in one dimension, coupled with a two–dimensional heat equation. The reaction–diffusion equation is eliminated by the temporary hypothesis that the gas mixture is dominated by argon, i.e. that all other gas species can be neglected.

To achieve the aforementioned reduction of dimension, all components of the growth apparatus are supposed to be cylindrically symmetric, and so is the distribution of absolute temperature. The quantities ρ_{gas} and $\vec{v}_{gas}$ are assumed to depend solely on the height z. Moreover, we do not take into account any non–zero component of velocity perpendicular to the z–direction.

We introduce the mean $\overline{T}_{gas}(z)$ of temperature at height z into the momentum balance equation of the gas phase, i.e. in equation (2.18b) $T_{gas}(r,z)$ is replaced by $\overline{T}_{gas}(z)$.

We do not take into account radiation inside the reactor at this stage.

The simplified balance equations inside the gas phase then take the following form:

$$\frac{\partial \rho_{gas}}{\partial t} + (v_{gas})_3 \frac{\partial \rho_{gas}}{\partial z} + \rho_{gas} \frac{\partial (v_{gas})_3}{\partial z} = 0, \tag{3.1a}$$

$$\rho_{gas} \frac{\partial (v_{gas})_3}{\partial t} + \rho_{gas} (v_{gas})_3 \frac{\partial (v_{gas})_3}{\partial z} + \frac{R}{M^{(\mathrm{Ar})}} \frac{\partial}{\partial z} \left(\rho_{gas} \overline{T}_{gas} \right) = \rho_{gas} (b_{gas})_3, \tag{3.1b}$$

$$\begin{aligned} \rho_{gas} R \frac{z^{(\mathrm{Ar})}}{M^{(\mathrm{Ar})}} \frac{\partial T_{gas}}{\partial t} + \frac{R z^{(\mathrm{Ar})}}{M^{(\mathrm{Ar})}} \rho_{gas} (v_{gas})_3 \frac{\partial T_{gas}}{\partial z} - \frac{1}{r} \frac{\partial}{\partial r} \left(r \kappa^{(\mathrm{Ar})}(T_{gas}) \frac{\partial T_{gas}}{\partial r} \right) \\ - \frac{\partial}{\partial z} \left(\kappa^{(\mathrm{Ar})}(T_{gas}) \frac{\partial T_{gas}}{\partial z} \right) + \frac{R}{M^{(\mathrm{Ar})}} \rho_{gas} T_{gas} \frac{\partial (v_{gas})_3}{\partial z} = 0. \end{aligned} \tag{3.1c}$$

3.2 Numerical Simulation of the Heat Transfer

So far, a discretized version of the heat transfer equation has been implemented in a form that is flexible with respect to boundary conditions and geometry changes. This is crucial, since the goal is to test different geometric set–ups of the growth apparatus numerically.

Time dicretization is done by a fully implicit Euler scheme that allows for a future coupling with the mass and momentum balance equations. A simple time step control mechanism is implemented to keep the solution change from one time step to the next in a given interval.

The space discretization employs a finite volume method based on the description in [Fuh97]. It has been slightly modified in order to account for the cylindrical symmetry and to allow a more flexible handling of boundary and transition conditions.

The discrete mesh is constructed using a grid generator which is adapted to the case of a domain consisting of rectangular patches.

The resulting nonlinear system of equations is solved via a Newton–Krylov method.

Both the grid generator and the nonlinear solver are taken from the PDELIB program package that is being developed at the WIAS Berlin.

3.3 Numerical Results

We exemplarily compare two numerical simulations of the time evolution of the temperature distribution inside the reactor. The two simulations use slightly different geometric configurations of the reactor. Both simulations start out with a homogeneous temperature distribution at room temperature and then are heated at the outer vertical rim of the graphite side of the reactor. The heating process is simulated via an appropriate transient Dirichlet condition and goes up to some 2560 K. At the graphite rims of the holes in the centers of the top and bottom parts of the reactor the boundary condition accounts for the emitted radiation via the Stefan–Boltzmann law. At all other outer boundaries (i.e. the outer boundaries ambient to the insulation layer) we use homogeneous Neumann conditions.

Figure 2 depicts the geometry of the growth apparatus that was used for the first simulation shown in Figures 4–7. By using a bigger hole at the top of the growth apparatus than at its bottom, one achieves a higher temperature at the bottom of the crucible which is well–known to be desirable for the growth process. The set–up of the second simulation differs from the first in that it uses a thinner insulation layer at the top and bottom parts of the reactor (cf. Figures 8–11).

The fixed non–uniform mesh is depicted in Figure 3.

Owing to the cylindrical symmetry of the problem, the actual computations take place only on the right–hand side of the reactor. For the reader's convenience the results have been reflected through the $r = 0$ line, so that the whole growth apparatus can be shown in the pictures.

For both numerical experiments we discuss three temporal snapshots, the first at 42.00 s, the second at 1786 s and the third at 5000 s. Figures 4–6 and Figures 8–10 provide the corresponding pictures with the temperature

isolines appearing in steps of 100 K. After 5000 seconds a quasi–stationary state is reached, and for each experiment we give another picture where the temperature isolines

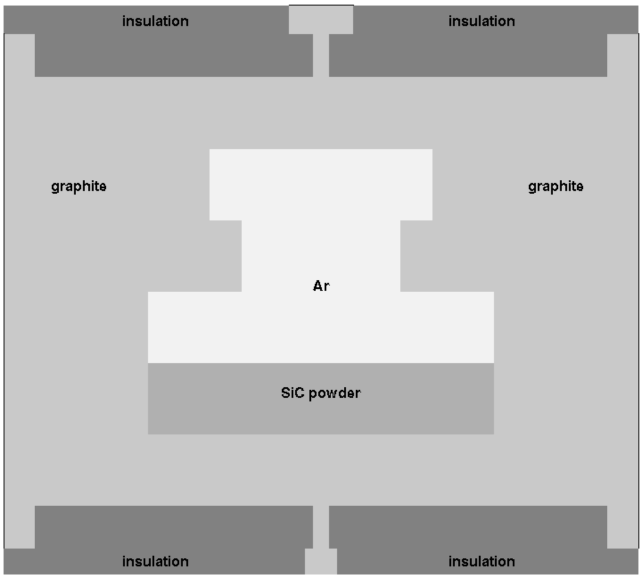

Figure 2: geometric set–up of the reactor

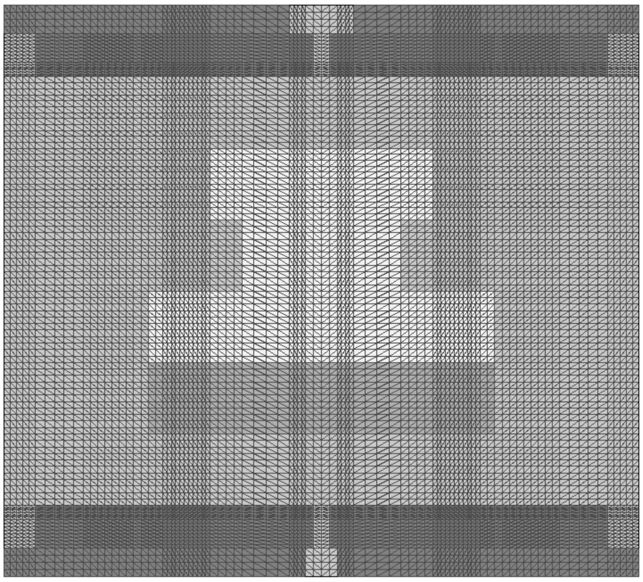

Figure 3: discretization of the spatial domain into non–obtuse triangles

appear in steps of merely 5 K, in order to give a more detailed view of the temperature field inside the actual growth chamber (cf. Figures 7 and 11).

While in Figures 4 and 8 there is virtually no noticeable difference in the temperature fields inside the growth chamber, the influence of the thinner insulation layer starts to take its toll in Figure 9 as compared to Figure 5. The thicker insulation slows down the heating process in the top and bottom parts of the reactor resulting in a considerably lower temperature at the graphite hole (note that the value of the minimal temperature T_{min} in Figure 5 is almost 600 K lower than the value of T_{min} in Figure 9). The order of magnitude of this difference in the minimal temperatures persists throughout the rest of the experiments as can be seen by comparing the minimal temperatures of the stationary states.

As the systems evolve further from the intermediate states depicted in Figures 5 and 9,

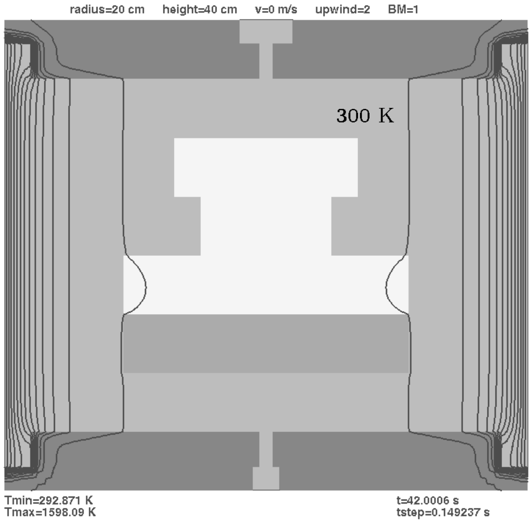

Figure 4: 1st experiment, 1st stage

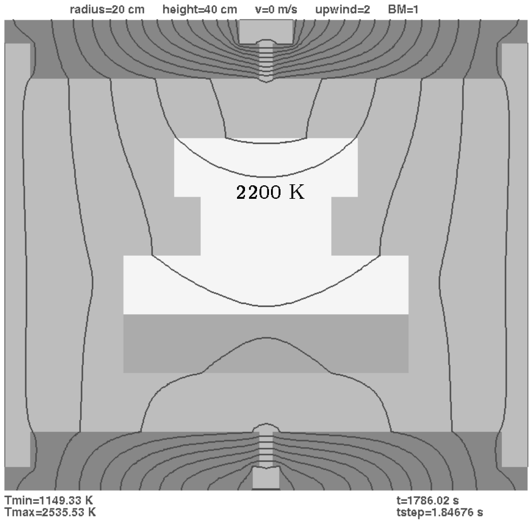

Figure 5: 1st experiment, 2nd stage

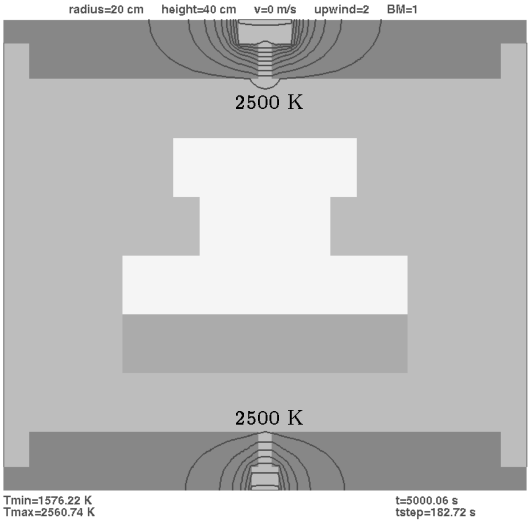

Figure 6: 1st experiment, 3rd stage, coarse isolines

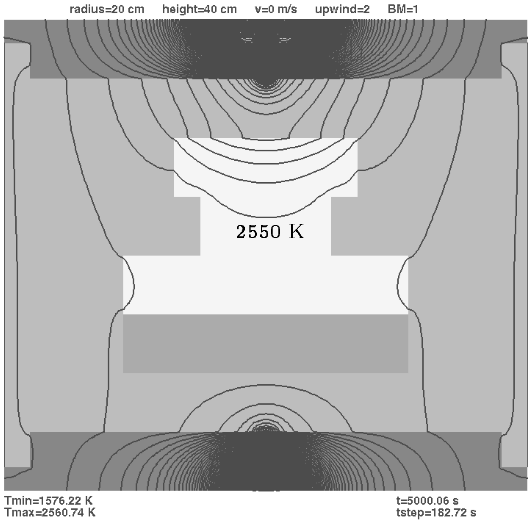

Figure 7: 1st experiment, 3rd stage, fine isolines

respectively, the temperatures at the horizontal boundaries of both set–ups reach levels at which the heat loss via radiation becomes more and more effective. By keeping the heat away from the radiating graphite hole, the thicker insulation layer of the first experiment hinders the heat loss of the reactor to the surrounding media. Thus the crucible is warmer for the first experiment.

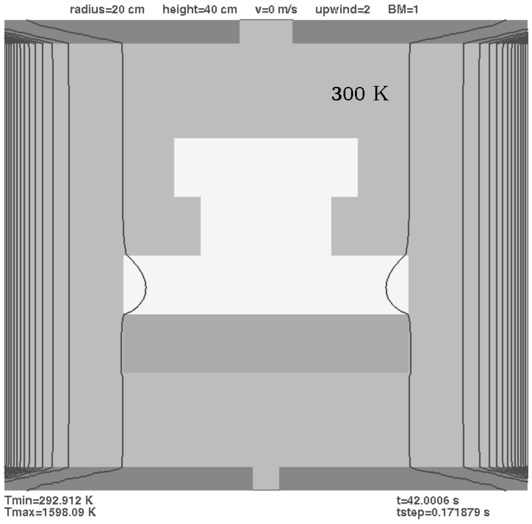

Figure 8: 2nd experiment, 1st stage

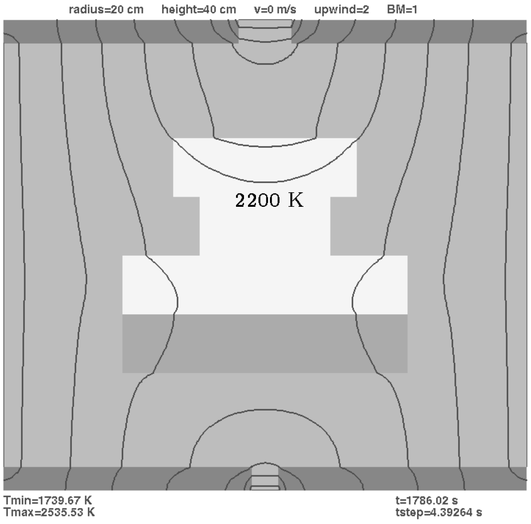

Figure 9: 2nd experiment, 2nd stage

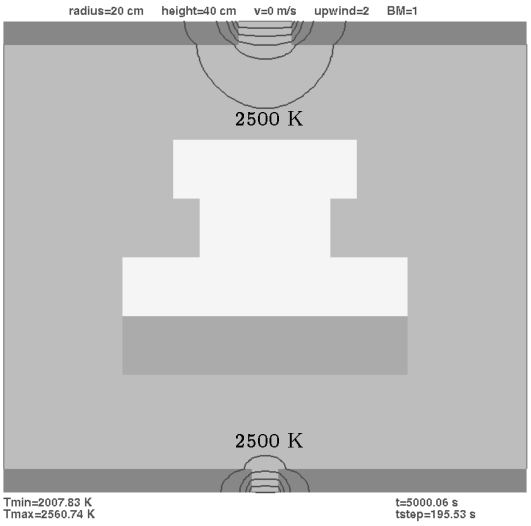

Figure 10: 2nd experiment, 3rd stage, coarse isolines

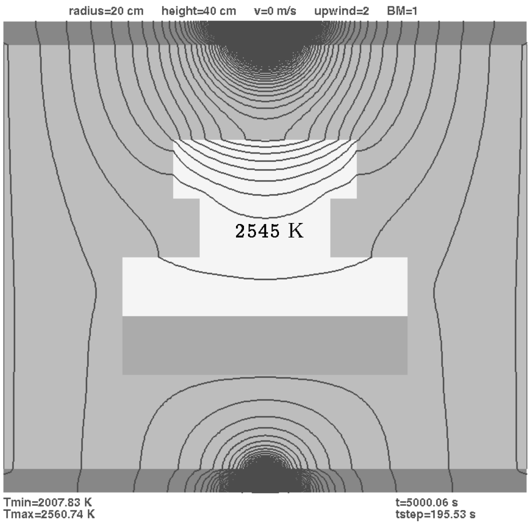

Figure 11: 2nd experiment, 3rd stage, fine isolines

References

[Fuh97] J. Fuhrmann. On numerical solution methods for nonlinear parabolic problems. In *Modeling and Computation in Environmental Sciences*, volume 59 of *Notes on Numerical Fluid Mechanics*, pages 170–180. Vieweg, Braunschweig/Wiesbaden, 1997.

[Har95] G. L. Harris, editor. *Properties of Silicon Carbide*. Institution of Electrical Engineers, INSPEC, London, 1995.

[HHW+95] D. Hofmann, M. Heinze, A. Winnacker, F. Durst, L. Kadinski, P. Kaufmann, Y. Makarov, and M. Schäfer. On the sublimation growth of SiC bulk crystals: development of a numerical process model. *Journal of Crystal Growth*, 146:214–219, 1995.

[Ins97] Institut für Kristallzüchtung, Berlin. Private communication, 1997.

[Kon95] A. O. Konstantinov. Sublimation growth of SiC. In Harris [Har95], chapter 8.2, pages 170–169.

[Lil93] S. K. Lilov. Study of the equilibrium processes in the gas phase during silicon carbide sublimation. *Material Science and Engineering*, B21:65–69, 1993.

[PBD+96] M. Pons, E. Blanquet, J. M. Dedulle, I. Garcon, R. Madar, and C. Bernard. Thermodynamic heat transfer and mass transport modelling of the sublimation growth of silicon carbide crystals. *J. Electrochem. Soc.*, 1996.